Rubio Rubio, Marinao… et al. (2018) Dripping dynamics and transitions at high Bond numbers, *International Journal of Multiphase Flow*, v. 104, pp.: 206-213.

DOI: https://doi.org/10.1016/j.ijmultiphaseflow.2018.02.017

Dripping dynamics and transitions at high Bond numbers

Mariano Rubio-Rubio[a,*], Paloma Taconet[b], Alejandro Sevilla[b]

[a] *Área de Mecánica de Fluidos, Departamento de Ingeniería Mecánica y Minera, Universidad de Jaén, Campus de las Lagunillas, 23071 Jaén, Spain*
[b] *Departamento de Ingeniería Térmica y de Fluidos, Universidad Carlos III de Madrid, Avda. de la Universidad 30, 28911 Leganés, Spain*

Abstract

We report experiments on the dripping dynamics and jetting transitions that take place when a liquid is injected vertically downwards at a constant flow rate, for wide ranges of the liquid viscosity and injector radius. We explore values of the Bond number significantly larger than in previous works, revealing the existence of period-2 dripping regimes with satellite formation that do not exist at small Bond numbers. In addition, we quantify the influence of liquid viscosity on the hysteresis associated with the dripping-jetting transition, that had previously been studied only for the particular case of water.

Keywords: Dripping, Jetting, Transition, Hysteresis, P2S regime

1. Introduction

Drop formation is a phenomenon present in nature, everyday life situations, industrial processes and medical, pharmaceutical and food applications (see e.g. Barrero and Loscertales, 2007; Eggers and Villermaux, 2008; Rodríguez-Rodríguez et al., 2015; Anna, 2016, and references therein). Fiber spinning (Pearson and Matovich, 1969; Stokes et al., 2014), electro spinning (Doshi and Reneker, 1995; Loscertales et al., 2002), or coflows (Gañán-Calvo, 1998; Gordillo et al.,

*Corresponding author
Email addresses: mrubio@ujaen.es (Mariano Rubio-Rubio), alejandro.sevilla@uc3m.es (Alejandro Sevilla)

2014; Evangelio et al., 2016) are examples of techniques widely used to stretch a liquid jet with the purpose of generating either tiny threads, or small drops with sizes significantly smaller than that of the injector. In addition, gravity can also be used as the stretching mechanism when a liquid is injected though a vertically orientated tube, if the flow rate is above a certain threshold (Clanet and Lasheras, 1999; Ambravaneswaran et al., 2004; Rubio-Rubio et al., 2013; Chakraborty et al., 2016). Below this jetting threshold, drops start growing at the outlet until the surface tension forces cannot longer balance their weight, and the pinch-off takes place, in a repetitive process known as *dripping regime*. As an example, Figure 1 shows the evolution of a pendant drop of 20 cSt polydimethylsiloxane (PDMS) oil, issuing from a tube of radius $R = 1.75$ mm at a constant flow rate $Q = 11$ ml/min.

Not only micron- and sub-micron-sized drops are of interest in applications. Pharmaceutical and alimentary industries face the problem of accurately dispensing doses of liquids with different properties (Chen, 2009). In addition, millimetric drops are routinely used for the characterisation of fluid-fluid interfaces. For instance, in the drop weight method, the static equilibrium between surface tension forces and the weight of a pendant liquid drop allows to extract the surface tension coefficient. In fact, in many practical applications, the inertia of the flow is not negligible, and its competition with the gravitational and surface tension forces may lead to chaotic behaviours, depending on the damping effect of the liquid viscosity. The simplest and most common example is a dripping faucet, which has been studied as a paradigm of chaotic system for many years (Shaw, 1984). For instance, Coullet et al. (2005) proposed a mechanical explanation for this chaotic behaviour through modelling and numerical simulations.

In the inviscid limit, drop formation was studied numerically by Schulkes (1994) using an axisymmetric boundary integral method. Taking advantage of the development of several one-dimensional (1D) model equations, the first attempts to simulate the formation of viscous drops at a very reduced computational cost dealt with the quasi-steady growth of the droplet (Eggers and

Dupont, 1994; Brenner et al., 1997). The drop formation process at a nonzero Weber number was thoroughly studied in the works of Prof. Basaran's group, both from the numerical and the experimental points of view, e.g. in the work of Wilkes et al. (1999) where the phenomenon is explored for wide ranges of the governing parameters. Later on, to show the capabilities and limitations of the 1D model, Ambravaneswaran et al. (2002) compared their results with simulations of the axisymmetric Navier-Stokes equations, finding that the agreement between the two models is remarkably good, especially when surface tension forces are dominant.

For small enough flow rates, main droplets as well as tiny satellite drops are formed periodically. As the flow rate is increased, satellites are no longer present, giving way to a period-1 dripping regime without satellite droplets (Zhang and Basaran, 1995; Zhang, 1999; Ambravaneswaran et al., 2002). If the flow rate is further raised, the transition to jetting takes place. Depending on the liquid viscosity, this transition can be preceded by more complex regimes, namely period-2, period-4, chaotic dripping etc. as mentioned above.

Ambravaneswaran et al. (2004) studied the effect of viscosity in the transition from dripping to jetting by numerically simulating the 1D equations. Their work revealed that, in a liquid with high enough viscosity, the dripping to jetting transition takes place without exhibiting intermediate chaotic dripping regimes, otherwise present in the case of low viscosity ones (Clanet and Lasheras, 1999; Coullet et al., 2005). In addition, and making use of simple scaling arguments, Ambravaneswaran et al. (2004) derived criteria to predict the transition to jetting. In a more extensive work, accompanied by experiments, Subramani et al. (2006) characterised the dripping regimes through bifurcations and phase diagrams, showing the high complexity of the phenomena when varying the governing parameters. However, all these works were performed at small Bond numbers, $Bo \leq 0.5$, far below the values studied in the present study.

As a natural continuation of the work by Rubio-Rubio et al. (2013), where the important role of the injector diameter in the jetting-to-dripping transition was demonstrated, the main objective of this paper is to extend the works of Am-

bravaneswaran et al. (2004) and Subramani et al. (2006) to substantially higher values of the Bond number. The paper is structured as follows: in Section 2 we describe the flow configuration and the variables used for the experimental analysis. The results are presented an discussed in Section 3, addressing specifically: the dripping and jetting transitions, including the hysteresis of the forward and reverse processes, the classification of regimes in the governing parameter space, and the existence of satellite droplets. Finally, the conclusions are summarised in Section 4.

2. Problem description

To characterise the dynamics of the dripping regimes as well as the jetting transition, the same parameters as in Ambravaneswaran et al. (2004) have been used. Consider a Newtonian liquid of constant and uniform properties, namely density ρ, kinematic viscosity ν and surface tension coefficient σ issuing from a capillary tube of radius R, at a constant flow rate Q. In the presence of the gravitational acceleration g, and in a quiescent surrounding atmosphere at pressure p_a, the drops growing and detaching from the injector outlet can be characterised by the volume of the detached drop V_d, the volume of the liquid that remains pending attached to the outlet V_p, and the limiting length L_d, defined as the distance from the tube at pinch-off. The definition of the relevant variables can be observed in Figure 1.

The experimental setup was the same as the one used in Rubio-Rubio et al. (2013), where the jetting to dripping transition was experimentally studied, and therefore it is also similar to those used in previous studies of jet and drop formation (Wilkes et al., 1999; Subramani et al., 2006). Basically, it consists of a vertical capillary tube of radius R through which different PDMS silicone oils from Sigma-Aldrich are injected at a constant flow rate, thanks to the use of a Harvard Apparatus PhD Ultra syringe pump. The experimental images are acquired using a Red Lake Motion Pro X high-speed camera. Both the injector and the camera are mounted on vibration-isolation table and enclosed

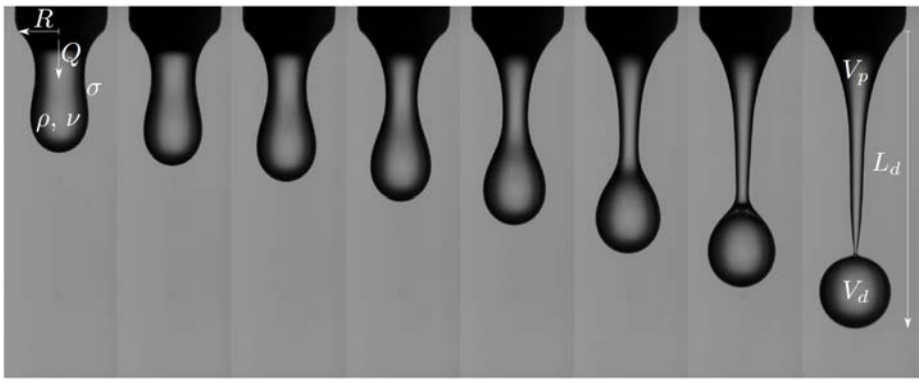

Figure 1: Sequence of images showing the evolution of a pendant drop of PDMS silicone oil of kinematic viscosity $\nu = 20$ cSt, injected at a constant flow rate $Q = 11$ ml/min through a tube of radius $R = 1.75$ mm, and variables used for the analysis of the experiments. The time interval between two consecutive frames is 6 ms

within a chamber to avoid ambient disturbances. The liquid is supplied through stainless steel tubes whose outlet is sharpened, so that the contact line is pinned at the inner diameter, avoiding the existence of two different radii to define the injection conditions. The inner radii of the capillary tubes were between 1.0 and 3.25 mm, with a length-to-diameter ratio large enough to ensure a fully developed velocity profile at the exit plane. The properties of the different liquids used in the present work can be found in Table 1.

The governing parameters of the experiments are the liquid properties ρ, ν and σ, the injector size R and the injection flow rate Q, apart from the gravitational acceleration g. In dimensionless terms, the dripping and jetting dynamics can be described through the values of three parameters, namely the Bond, $Bo = \rho g R^2/\sigma$, Weber, $We = \rho U^2 R/\sigma$, and Kapitza, $\Gamma = 3\nu(\rho^3 g/\sigma^3)^{1/4}$, numbers defined as in Rubio-Rubio et al. (2013), with $U = Q/(\pi R^2)$ the mean exit velocity. Traditionally, the Ohnesorge number $Oh = \eta/\sqrt{\rho R \sigma}$, being $\eta = \rho\nu$ the dynamic viscosity of the liquid, has been used in these type of studies. Nevertheless, the use of Γ, which is similar to the Morton number $Mo = g\nu^4\rho^3/\sigma^3$, often used in the bubble literature, results a more natural choice, because its value depends only on the liquid properties for a given value of g, and not on

ν [mm^2 s^{-1}]	ρ [kg m^{-3}]	σ [mN m^{-1}]	Γ
2	833	18.3	3.31×10^{-2}
5	915	19.7	8.40×10^{-2}
10	935	20.1	1.68×10^{-1}
20	950	20.6	3.34×10^{-1}
50	960	20.8	8.36×10^{-1}

Table 1: Properties at 25 ^{0}C of the Sigma-Aldrich silicon oils used in the present study. The last column represents the Kapitza number, $\Gamma = 3\nu(\rho^3 g/\sigma^3)^{1/4}$, computed using a value of $g = 9.81$ ms^{-2}.

the length scale. Thus, a change in the value of Γ implies only a variation of the working fluid. In contrast, when using Oh as a governing parameter, its change can be associated either with a variation of the liquid properties or a change in the injector size. This fact can be readily observed either from the definition of Oh or from the relation $Oh = Bo^{1/4}/(3\Gamma)$.

3. Results

The rich nonlinear dynamics of the dripping regime can be appreciated by observing the wide diversity of responses present in a dripping faucet when the governing parameters are varied. The results presented in Figure 2(a) show an example of periodic dripping, in which all the main drops detached from the tube are of equal size and the pinch-off occurs at the same point. This fact means that there is a single value of both L_d/R and of V_d/V_p for a given value of We. This regime is known in the literature as period-1 or P1, and constitutes the simplest possible dripping behaviour. In contrast, if the drops alternatively detach at two different lengths from the outlet, with two different shapes respectively, the regime is known as period-2, or P2. There are also examples of odd-dynamics, such as period-3 regime or P3, reported in the literature. In addition, apart from these periodic regimes, the ejected drops may exhibit a chaotic behaviour, CD, with different volumes and detachment lengths without

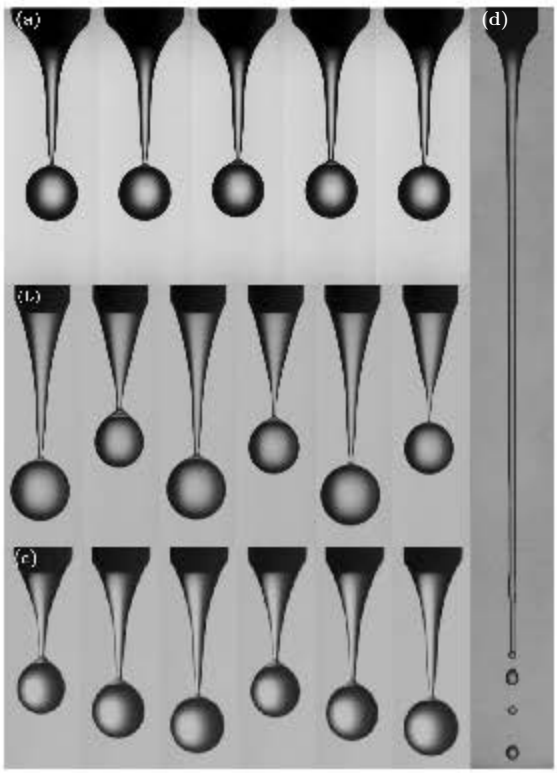

Figure 2: Examples of consecutive drops in the case of P1 regime (a), P2 (b), P3 (c) and jetting (d). The values of the governing parameters in each case are $Bo = 2.2$, $We = 1.11 \times 10^{-2}$, $\Gamma = 0.17$ (a), $Bo = 0.7$, $We = 6.65 \times 10^{-2}$, $\Gamma = 0.33$ (b), $Bo = 1.0$, $We = 4.69 \times 10^{-2}$, $\Gamma = 0.17$ (c) and $Bo = 2.2$, $We = 2.11 \times 10^{-2}$, $\Gamma = 0.084$ (d).

exhibiting any periodicity.

The periodic regimes P1, P2 and P3 described in the previous paragraph are depicted in Figures 2(a), (b) and (c) respectively, while a faucet in the jetting regime is shown in Figure 2(d), for illustrative purposes. Figure 3(a) shows an example of chaotic dripping while in Figure 3(b) the values of the dimensionless detachment length for i consecutive droplets are represented, revealing the chaotic behaviour of this regime. The values of the governing parameters in each case can be found in the corresponding figure captions.

The presence of satellite droplets will be specifically addressed in Section 3.3. Therefore, in the dripping regimes mentioned above, and summarised in the

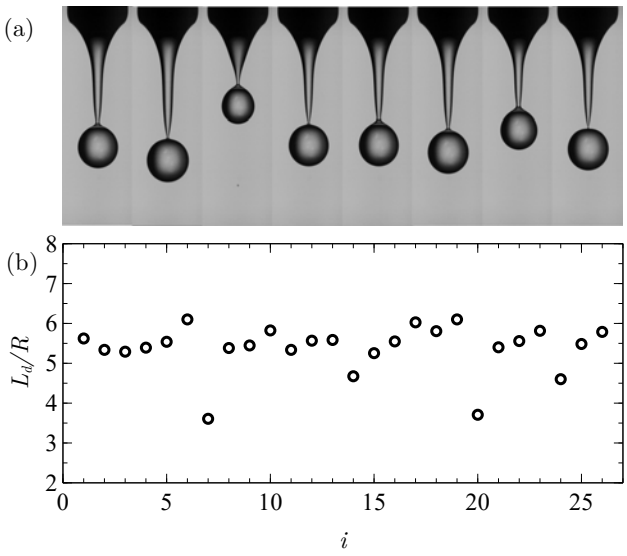

Figure 3: Consecutive drops in the chaotic dripping regime (a) and values of the dimensionless limiting length (b) for $Bo = 2.2$, $We = 1.46 \times 10^{-2}$, $\Gamma = 0.084$.

phase maps presented in the following sections, there is no explicit differentiation between cases with and without satellites, provided that the main droplets exhibit the same behaviour.

3.1. Dripping to jetting transition. Phase diagrams at constant Kapitza number

There are many examples in the literature in which qualitative or ad-hoc criteria are used to decide when the transition to jetting takes place. As an example, Clanet and Lasheras (1999) considered that the jetting regime occurred when the value of the limiting length accomplished the criterion $L_d/R \sim 20$. Nevertheless, this approach, which is valid in the case of water in a first approximation, fails when the viscosity of the liquid increases due to the formation of very long ligaments in the dripping regime. Therefore, the criterion used in the present work follows that of Ambravaneswaran et al. (2004): the transition to jetting can be easily identified because the values of L_d/R and V_d/V_p undergo sudden and large changes at the same time, as clearly evidenced in Figure 4. The detachment length increases abruptly at a value of $We = We_j$, as can be

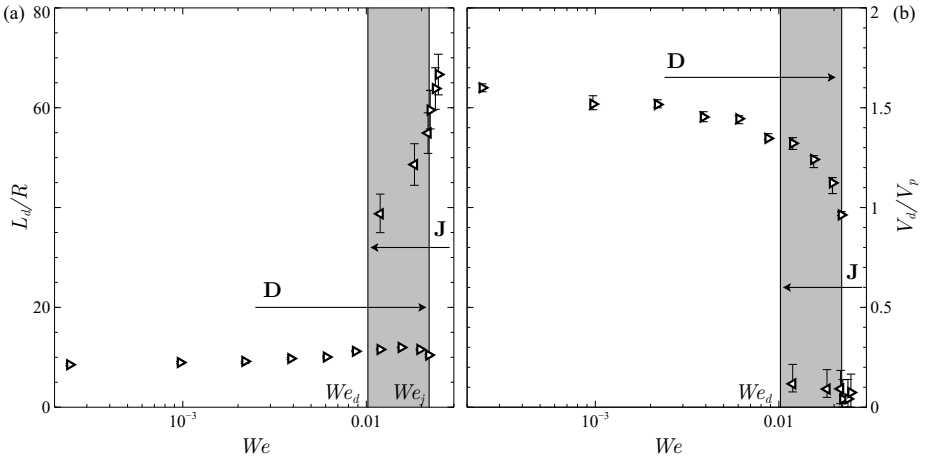

Figure 4: Nondimensional limiting length L_d/R (a) and detached to pendant volume ratio V_d/V_p (b) as functions of We, for $Bo = 1.39$ and $\Gamma = 0.84$. The vertical lines represent the critical values of We at which the transition from dripping to jetting, We_j, and from jetting to dripping, We_d, take place. Hysteresis exists in the shaded region, where pointing left triangles have been used to represent the experimental results.

appreciated in Figure 4(a), while the volume ratio suddenly decreases at the same Weber number We_j, as represented in Figure 4(b). Once a jet is formed, the flow rate can be reduced below the value of We_j prior to recovering the dripping regime (Clanet and Lasheras, 1999). Thus, the jetting to dripping transition occurs at a Weber number $We_d < We_j$. The shaded region in the figure thus represents the hysteresis associated with the two transitions.

The same analysis has been performed for different values of Bo, as summarised in Figure 5. The shadowed zones in Figure 5 correspond again to the hysteresis of the transition for each value of Bo, but in these cases they have been plotted only either in Figure 5(a) or (b), to avoid the overlapping of the hysteretic regimes, and thus to ease the reading of the figures. The error bars have been omitted for clarity, since the uncertainties are similar to those already presented in Figure 4. It should be pointed out that this hysteresis had not been previously quantified for any liquid different from water (Clanet and Lasheras, 1999).

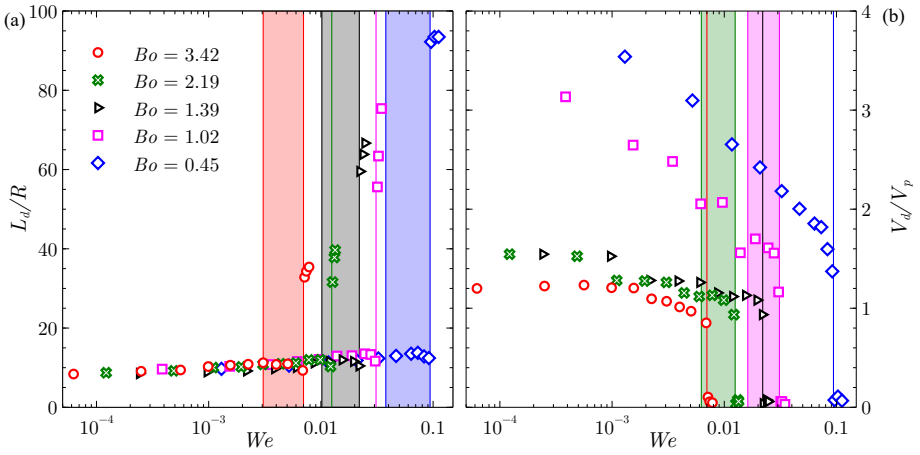

Figure 5: (Colour online) Dimensionless limiting length L_d/R (a) and volume ratio V_d/V_p (b) as functions of Weber number We, for $\Gamma = 0.84$ and several values of Bo. The vertical lines represent the transition to jetting, and the shaded areas correspond to the hysteresis associated with the two transitions, shown for each Bond number only either in panel (a) or (b) for clarity.

Figure 6(a) shows the experimental value of We_j and the hysteresis present in the transition as functions of Bo, for a given liquid, that is, for a fixed value of $\Gamma = 0.84$ corresponding to the silicone oil of kinematic viscosity $\nu = 50$ cSt. The boundary represented by the symbols $\triangle$, divides the Bo-We plane into two regions, yielding a phase map in which points above the curve correspond to a jetting regime, labelled J in the figures. Below this critical curve, in the zone labelled P1, the behaviour corresponds with the period-1 dripping regime. Thus, this is an example of *simple dynamics*, as defined in Subramani et al. (2006), being the possible responses either P1 or J. The hysteresis can also be observed in Figure 6(a), where the symbols $\triangledown$ represent the boundary for the jetting to dripping transition. The shaded area shows the hysteretic region of the Bo-We parameter plane where the regime is P1 when increasing the flow rate. However, if the jet is previously formed, and then the value of We is decreased, the corresponding regime is jetting inside the shaded area.

Figure 6(b) represents another phase map in the Bo-We plane for a smaller

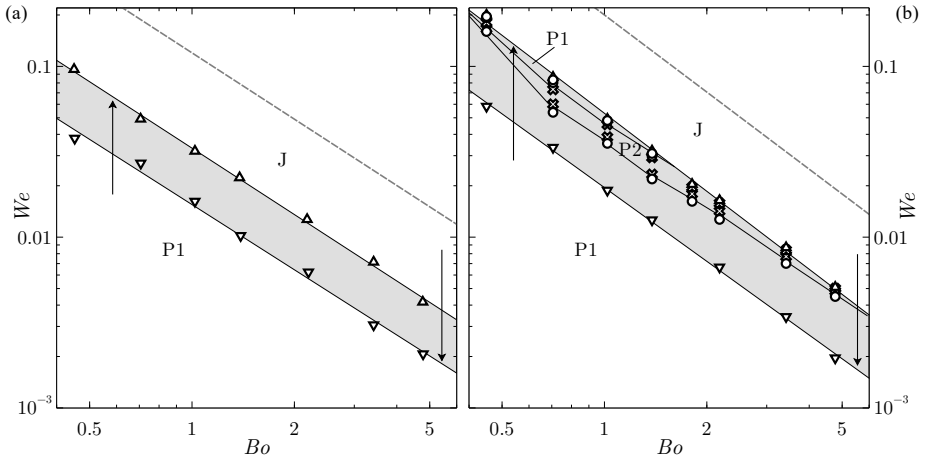

Figure 6: Phase maps showing the regimes in the (Bo, We) parameter plane when $\Gamma = 0.84$ (a) and $\Gamma = 0.33$ (b). The symbols represent the experimental transition points. The regions are labelled P1 for period-1 dripping, P2 for period-2 dripping and J for jetting. The shaded areas correspond to the hysteresis of the dripping to jetting transition, marked with the symbol $\triangledown$. The dashed lines show the fitted power law $We_j \sim Bo^{-n}$, with $n = 1.3$ (a) and $n = 1.5$ (b).

value of $\Gamma = 0.33$, associated with a liquid of kinematic viscosity $\nu = 20$ cSt. The responses present in this case are referred to as *complex dynamics* in Subramani et al. (2006). Indeed, there exists another regime besides the P1 and J behaviours. Specifically Figure 6(b) reveals that there is a region delimited by crosses in which the observed regime is P2. In agreement with the results of Ambravaneswaran et al. (2004), the P2 zone is found when increasing the Weber number right after P1. It is also worth pointing out that there is a narrow P1 zone before the transition to jetting for small Bond numbers, as reported in Subramani et al. (2006) for a value of $Bo = 0.3$. The hysteresis of the jetting to dripping transition is represented as well in Figure 6(b). It can be appreciated that the decrease in We_d leads to P1 regimes after the dripping transitions. Hence, if the flow rate is decreased starting from a formed jet, the whole period-2 zone is affected by the hysteresis, so that the P2 regime does not even appear when the value of We is decreased.

Making use of simple scaling arguments, Ambravaneswaran et al. (2004) provided criteria to predict the dripping to jetting transition by comparing the different time scales that appear in the problem. In particular, they argued that the critical Weber number We_j varies with the Ohnesorge number through a power law, being $We_j \sim \mathcal{O}(1)$ for $Oh \ll 1$; $We_j \sim Oh^{-6}$ for $Oh \sim 1$ and $We_j \sim Oh^{-2}$ for $Oh \gg 1$. Nevertheless, these scalings, which are in agreement with the simulations presented in Ambravaneswaran et al. (2004) and Subramani et al. (2006) for small Bond numbers, are unable to capture the experimental transitions reported herein for larger values of Bo. The results shown in Figure 6 can be fitted to a power law $We_j \sim Bo^{-n}$, obtaining $n \approx 1.3$ in the case of $\Gamma = 0.83$, and $n \approx 1.5$ when $\Gamma = 0.33$. These power laws are represented with dashed lines in Figure 6. This strong dependence on the Bond number for a fixed value of Γ suggests that the scaling laws previously proposed in the literature must be reconsidered to account for larger values of Bo. In fact, making use of the relationship $\Gamma = 3OhBo^{1/4}$, the fitting $We_j \sim Bo^{-3/2}$ for the silicon oil of $\nu = 20$ cSt yields $We_j \sim Oh^6$, in marked contradiction with the scaling law proposed in Ambravaneswaran et al. (2004) for intermediate Ohnesorge numbers, namely $We_j \sim Oh^{-6}$.

Let us now present a scaling argument for the transition behaviour observed in our experiments at large Bond numbers. In the dripping regime at small Bond numbers, the size of the droplets is much larger than the injector radius. In contrast, when $Bo \gtrsim 1$, the radius of the detached drop is similar to that of the nozzle. Nevertheless, a more accurate estimation is needed to develop a new scaling law for the jetting transition. Villermaux et al. (2013) showed that, when $Bo \gtrsim 1$, the detached droplet radius scales with the capillary length $l_\sigma = \sqrt{\sigma/(\rho g)}$. As there are no other external forces apart from gravity, we can consider that the drops are in free fall. Thus, after falling a distance of order l_σ, their velocity is of order $v_f \sim \sqrt{g l_\sigma}$. Now, consider a dripping faucet from which droplets are continuously detaching. As can be easily observed if increasing gradually the flow rate in a tap, when the flow rate is increased the frequency of detachment increases and therefore, the space between two

consecutive droplets is reduced. The latter argument suggests a picture of the transition to jetting as the moment in which all the detached droplets of radius $r_d \sim l_\sigma$, falling at a speed $\sqrt{gl_\sigma}$ are so close to each other that they coalesce in a continuous liquid column, giving way to jet formation. In the latter critical conditions, the liquid issued by the injector accomplishes $U^2 R \propto v_f^2 l_\sigma$, leading to $We_j \propto Bo^{-3/2}$, in fair agreement with the power laws shown in Figure 6. In our toy model the liquid viscosity is not accounted for, but in a first approximation the simple picture established in the present paragraph is able to explain the strong dependence of We_j on Bo, for values of $Bo \gtrsim 1$.

3.2. Phase diagrams at constant Bond number

To illustrate the effect of viscosity the results have also been represented in a Γ-We plane at a constant value of Bo. Figure 7(a) shows the results for the case $Bo = 1.0$, while $Bo = 2.2$ in Figure 7(b). In agreement with the results of Ambravaneswaran et al. (2004) and Subramani et al. (2006), it can be observed that decreasing the liquid viscosity leads to more complex dynamics. Thus, a region of chaotic dripping at small enough values of Γ can be found in Figure 7. In addition, it depicts that there exists a critical value Γ_c which divides the phase diagrams into two zones, one with simple dynamics for $\Gamma > \Gamma_c$ and other for $\Gamma < \Gamma_c$ where regimes other than P1 and J can be found. The existence of this critical value is clear since the dynamics change from *simple* to *complex* when decreasing the viscosity of the liquid. It is because of this reason that the viscosities of the liquids used for the experiments reported in this study are smaller than those considered in Rubio-Rubio et al. (2013). Note that larger values of Γ lead to simple phase maps qualitatively similar to that of Figure 6(a). It should be noticed that the representation of Γ_c for the two cases shown in Figure 7 is only qualitative, since its exact value lies within the experimental points. A more precise characterisation of the relationship $\Gamma_c(Bo)$ could be desirable, by means of new experiments or simulations.

The choice of $Bo = 1.0$ allows a comparison with the numerical results of Subramani et al. (2006), where a few computations are reported to illustrate

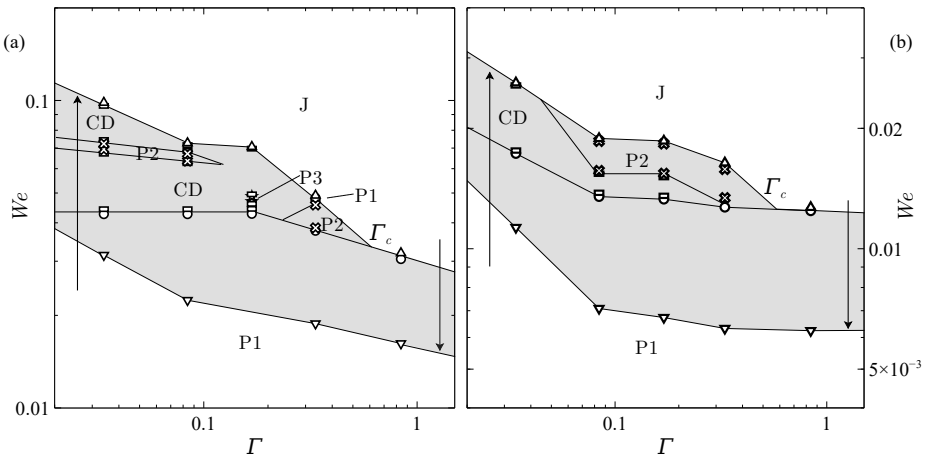

Figure 7: Phase maps showing the regimes present in the (Γ, We) parameter plane for $Bo = 1.0$ (a) and $Bo = 2.2$ (b). The symbols represent the experimental transition points. The regions are labelled P1 for period-1, P2 for period-2 and P3 for period-3 dripping. CD stands for chaotic dripping, and J for jetting. The shaded area corresponds to the hysteresis of the dripping to jetting transition.

the dynamics for $Bo \sim O(1)$. It should be highlighted that the value of $Bo \approx 0.96$ considered by Subramani et al. (2006), although high compared with the values $Bo \approx 0.3$ and $Bo \approx 0.5$ thoroughly studied in previous works, is still much smaller than the value of $Bo \approx 5$ reached in the present study. Figure 7(a) shows a small region of P3 dynamics, in fair agreement with the values $Bo = 0.97$, $We = 0.05$, $\Gamma = 0.3$ reported by Subramani et al. (2006).

As done before, the hysteresis of the jetting transition is also represented in figures 7(a) and (b). The shaded region corresponds to points of the Bo-We plane where the regime is jetting when decreasing the Weber number from a previously formed jet. It is clear from both figures that the hysteresis suppresses any complex response of the faucet when dripping is achieved by reducing the flow rate from the jetting regime.

3.3. Satellite drops

The experiments performed in the present work also allow to distinguish the cases in which there exist satellites between the main drops. The occurrence of

satellite drops has been previously analysed with different approaches. Using the VOF numerical method, Zhang (1999) derived a correlation for the limiting Weber number for satellites to exist, namely $WeBo^{0.3921} = 0.0125$. However, this correlation does not take into account the effect of liquid viscosity, due to the failure of the code by Zhang (1999) to converge at moderate to high values of the Ohnesorge number. In Ambravaneswaran et al. (2002), the authors performed 1D computations to depict the boundary of satellite formation when varying the value of Oh but, as previously mentioned, only for $Bo = 0.3$.

In a study of the viscous Savart sheet, Villermaux et al. (2013) performed dripping experiments at high Bond numbers to explain the bimodality of the droplet size distribution. In particular, by comparing the concomitant effects of viscosity, capillary destabilisation and the recoiling of the filament that appears after pinch-off, the authors provide an explanation both for the presence of one small satellite droplet per main drop, and for the ratio of the satellite to main drop size. The liquid used in their experiments corresponds to a value of $\Gamma = 2.19 > \Gamma_c$, therefore observing only simple dynamics. In their experiment they used a value of $Bo = 2.15$, with corresponding results in agreement with those presented in the previous sections.

Figure 8 shows the regions where satellite drops are present in the We-Bo plane for two different values of Γ. The shadowed areas correspond to experimental points of this study in which satellite formation is observed, and the dashed line is the correlation derived by Zhang (1999) through numerical simulations. The points from Subramani et al. (2006) are also included in the figure for completeness.

It is clear from Figure 8 that the increase of the injector radius leads to the presence of satellite droplets in regions different from P1. As an example, Figure 9 shows a new type of P2 regime that has been reported recently in a numerical study (Chakraborty et al., 2016), but not confirmed experimentally up to date. While Figure 2(b) depicts the classical period-2 regime without satellite droplets, the experiments performed in the present work reveal that if the Bond number is high enough, satellite droplets detach just behind the drop

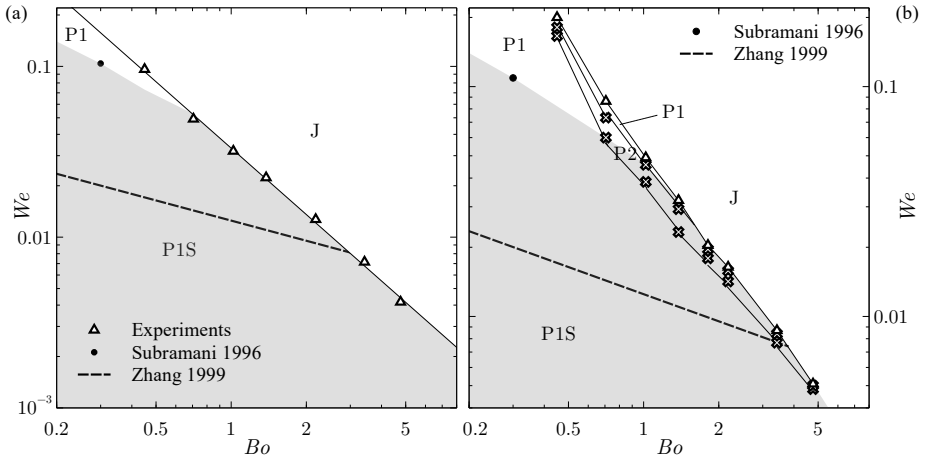

Figure 8: Existence of satellite drops in the (Bo, We) parameter plane (shaded areas) for $\Gamma = 0.84$ (a) and $\Gamma = 0.33$ (b). The results of Subramani et al. (2006) have been included with filled symbols, and the dashed line represents the correlation numerically derived by Zhang (1999).

that pinches-off at a larger distance from the outlet. This new regime, called P2S1, can be clearly observed in Figure 9(a) and in movie 1 of the supplementary material. Moreover, for still larger values of Bo, another kind of P2 regime takes place with satellite formation after each detachment of a main drop, referred to as P2S2 regime, and illustrated in Figure 9(b) and in movie 2 of the supplementary material. It should be pointed out that the presence of satellite droplets in period-2 dripping had not been reported before experimentally, since all the previous studies were done for values of the Bond number too small for the appearance of these regimes reported herein for the first time. Indeed, the P3 regime depicted in Figure 2(c) and found in the (Γ, We) parameter plane for $Bo = 1.0$ in Figure 7(a) actually is a regime with satellite droplets, as can be observed in movie 3 of the supplementary material. The presence of satellites in this period-3 regime was not mentioned in the work by Subramani et al. (2006), where the P3 appearance was numerically addressed.

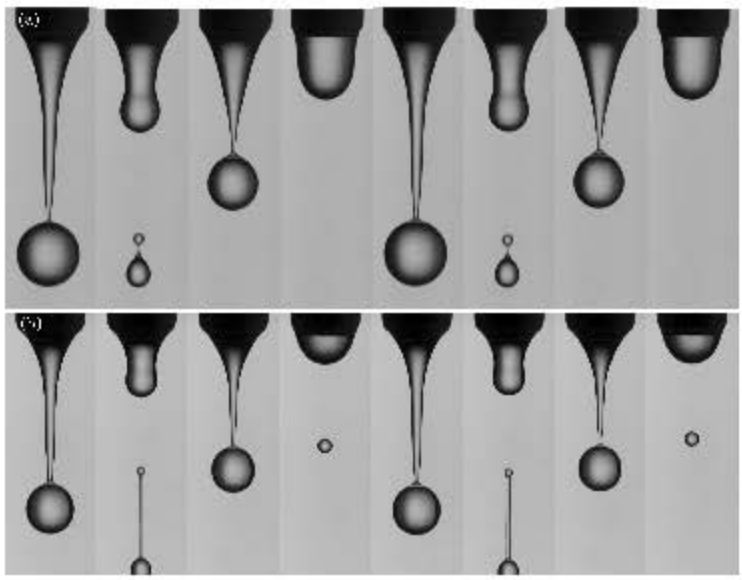

Figure 9: Example of satellites presence in period-2 regime, showing the case of P2S1 for $Bo = 1.38$, $We = 2.93 \times 10^{-2}$ and $\Gamma = 0.17$ (a) and P2S2 for $Bo = 2.2$, $We = 1.53 \times 10^{-2}$ and $\Gamma = 0.17$ (b).

4. Conclusions and future works

In this paper, we have revisited both the dripping dynamics and the transition to jetting experimentally, reaching values of the Bond number, Bo, significantly larger than in previous studies of drop formation. As suggested by Subramani et al. (2006), it has indeed been shown in the present work that larger injector sizes increase the complexity exhibited by a leaky faucet, to such an extent that the previous scaling laws (Ambravaneswaran et al., 2004) break down when the value of Bo varies in a wide range. This influence of the injector radius has been accounted for through a new scaling law for the transition to jetting in the limit of negligible viscous effects. Finding a scaling law that is also able to include the effect of liquid viscosity clearly deserves further theoretical effort. The comprehensive experimental work performed in the present work has been summarised through new phase diagrams, based on dimensionless parameters more adequate than those used in previous studies, using the

Kapitza number Γ, which depends only on the liquid properties, instead of the Ohnesorge number Oh. The phase maps reported herein could be improved by adding points in the regions where the dynamics is more interesting. This could be done either by means of numerical simulations (Chakraborty et al., 2016), or by performing new experiments, with the purpose of overcoming the limitations associated with the discrete experimental points reported in this study: smooth variations in the parameter space through experiments imply the need of an even more intensive experimental sweep than those already performed in this work. In addition, the hysteresis of the dripping to jetting transition has been quantified for the first time for working liquids different from water. In all the cases shown here, the regime present after the jetting to dripping transition was found to be P1, as a consequence of the hysteresis of the phenomenon. Finally, new regimes with satellite droplet formation, reported before only numerically (Chakraborty et al., 2016), have been found at high enough values of Bo. In particular, the existence of a period-2 regime with one satellite per double period for intermediate Bond numbers, and a period-2 regime with two satellites per double period for higher values of Bo.

Acknowledgements

The authors thank the financial support of the Spanish MINECO through projects no. DPI2011-28356-C03-02, no. DPI2014-59292-C03-01-P, no. DPI2015-71901-REDT and no. DPI2017-88201-C3-3-R. These research projects have been partly financed through European funds.

References

References

Ambravaneswaran, B., Subramani, H.J., Phillips, S.D., Basaran, O.A., 2004. Dripping-jetting transitions in a dripping faucet. Phys. Rev. Lett. 93, 034501.

Ambravaneswaran, B., Wilkes, E.D., Basaran, O.A., 2002. Drop formation from a capillary tube: Comparison of one-dimensional and two-dimensional analyses and occurrence of satellite drops. Phys. Fluids 14, 2606–2621.

Anna, S., 2016. Droplets and bubbles in microfluidic devices. Annu. Rev. Fluid Mech. 48, 285–309.

Barrero, A., Loscertales, I.G., 2007. Micro- and nanoparticles via capillary flows. Annu. Rev. Fluid Mech. 39, 89–106.

Brenner, M.P., Eggers, J., Joseph, K., Nagel, S.R., Shi, X.D., 1997. Breakdown of scaling in high Reynolds number droplet fission. Phys. Fluids 9, 1573–1590.

Chakraborty, I., Rubio-Rubio, M., Sevilla, A., Gordillo, J.M., 2016. Numerical simulation of axisymmetric drop formation using a coupled level set and volume of fluid method. Int. J. Multiphase Flow 84, 54–65.

Chen, X.B., 2009. Modeling and control of fluid dispensing process: A state of the art review. Int. J. Adv. Manuf. Technol. 43, 276–286.

Clanet, C., Lasheras, J.C., 1999. Transition from dripping to jetting. J. Fluid Mech. 383, 307–326.

Coullet, P., Mahadevan, L., Riera, C.S., 2005. Hydrodynamical models for the chaotic dripping faucet. J. Fluid Mech. 526, 1–17.

Doshi, J., Reneker, D.H., 1995. Electrospinning process and applications of electrospun fibers. J. Electrostatics 35, 151–160.

Eggers, J., Dupont, T.F., 1994. Drop formation in a one-dimensional approximation of the navier-stokes equation. J. Fluid Mech. 262, 205–222.

Eggers, J., Villermaux, E., 2008. Physics of liquid jets. Rep. Prog. Phys. 71, 036601.

Evangelio, A., Campo-Cortés, F., Gordillo, J., 2016. Simple and double microemulsions via the capillary breakup of highly stretched liquid jets. J. Fluid Mech. 804, 550–577.

Gañán-Calvo, A.M., 1998. Generation of steady liquid microthreads and micron-sized monodisperse sprays in gas streams. Phys. Rev. Lett. 80, 285–288.

Gordillo, J.M., Sevilla, A., Campo-Cortés, F., 2014. Global stability of stretched jets: conditions for the generation of monodisperse micro-emulsions using coflows. J. Fluid Mech. 738, 335–357.

Loscertales, I.G., Barrero, A., Guerrero, I., Cortijo, R., Marquez, M., Gañán-Calvo, A.M., 2002. Micro/nano encapsulation via electrified coaxial liquid jets. Science 295, 1695–1698.

Pearson, J.R.A., Matovich, M.A., 1969. Spinning a molten threadline. I&EC fundamentals 8, 605–609.

Rodríguez-Rodríguez, J., Sevilla, A., Martínez-Bazán, C., Gordillo, J.M., 2015. Generation of microbubbles with applications to industry and medicine. Annu. Rev. Fluid Mech. 47, 405–429.

Rubio-Rubio, M., Sevilla, A., Gordillo, J.M., 2013. On the thinnest steady threads obtained by gravitational stretching of capillary jets. J. Fluid Mech. 729, 471–483.

Schulkes, R.M.S.M., 1994. The evolution and bifurcation of a pendant drop. J. Fluid Mech. 278, 83–100.

Shaw, R., 1984. The dripping faucet as a model chaotic system. Aerial Press, Santa Cruz, CA.

Stokes, Y.M., Buchak, P., Crowdy, D.G., Ebendorff-Heidepriem, H., 2014. Drawing of micro-structured fibres: circular and non-circular tubes. J. Fluid Mech. 755, 176–203.

Subramani, H.J., Yeoh, H.K., Suryo, R., Xu, Q., Ambravaneswaran, B., Basaran, O.A., 2006. Simplicity and complexity in a dripping faucet. Phys. Fluids 18, 032106.

Villermaux, E., Pistre, V., Lhuissier, H., 2013. The viscous Savart sheet. J. Fluid Mech. 730, 607–625.

Wilkes, E.D., Phillips, S.D., Basaran, O.A., 1999. Computational and experimental analysis of dynamics of drop formation. Phys. Fluids 11, 3577–3598.

Zhang, X., 1999. Dynamics of growth and breakup of viscous pendant drops into air. J. Colloid Sci. 212, 107.

Zhang, X., Basaran, O.A., 1995. An experimental study of dynamics of drop formation. Phys. Fluids 7, 1184.